Ocean Systems Engineering, *Vol. 14, No. 4 (2024) 315-330*
https://doi.org/10.12989/ose.2024.14.4.315

Computational simulation of compressible Newtonian flow past circular and square bluff bodies

Anas Al-Haboobi*[1], Ihssan A. Fadhel[2], Alaa A. Sharhan[3] and Alaa H. Al-Muslimawi[4]

[1]*Department of Postgraduate Studies, University of Kufa, Kufa, Iraq*
[2]*Ministry of Education, General Directorate of Education of Basrah, Basrah, Iraq*
[3]*Ministry of Education, General Directorate of Education; Baghdad/First Rusafa, Baghdad, Iraq*
[4]*Department of Mathematics, College of Sciences, University of Basrah, Basrah, Iraq*

(Received February 12, 2024, Revised April 7, 2024, Accepted April 12, 2024)

Abstract. In this paper, we concerned with the study of an essential and intriguing aspect of fluid with bluff bodies. Mainly, the viscosity is highlighted on the effect of bluff circular and square bodies that immersed in a compressible Newtonian fluid. An accurate Taylor-Galerkin/Pressure-Correction (TG/PC) algorithm is employed to address this phenomenon computationally. In addition, and given the compressible nature of the fluid, determination of density requires to use specific state equation, which is incorporated with the governing fluid equations. The impact of viscosity (μ) on various components, encompassing velocity (v), pressure (p), and density (ρ) represents the main aim in this investigation. Furthermore, a detailed comparison between compressible and incompressible fluids based on the distinct effect arising from bluff bodies of circular or square shapes is provided. The findings emphasized on the reliability and accuracy of the numerical method and aligning consistently with physical phenomena, and its compatibility with the previous research.

Keywords: compressible flow; density; finite element method; Newtonian flow; Taylor-Galerkin/Pressure-Correction method; viscosity

1. Introduction

Study of fluid flow past cylindrical or square bodies represents an importance issue in engineering applications, in which many experimental and computational studies have been conducted. Vortex shedding, turbulence, and flow separation are just a few of the notable physical phenomena that are seen in the flow patterns surrounding these bodies. Numerous fluid mechanical characteristics, including lift forces, drag and pressure coefficients brought about by induced forces, are significantly impacted by these phenomena, particularly the processes controlling vortex shedding and its suppression Bimbato *et al*. (2011). The drag force, which is partly affected by the fluid's viscosity, is the resistance that a solid body experiences when flowing in a certain direction.

In general, the fluid flows over obstacles or moves over man-made or natural bodies is known as fluid flowing over a bluff body Choi *et al.* (2008). Recently, many researchers have made great

*Corresponding author, Ph.D., E-mail: anasm.ali@uokufa.edu.iq

http://www.techno-press.org/?journal=ose&subpage=7 ISSN: 2093-6702 (Print), 2093-677X (Online)

efforts in learning more about how bluff bodies behave in fluid flow has grown. Griffin and Hall (1991) show that when a bluff body is put in an incident mean flow with a periodic component overlaid onto it, the phenomena of vortex shedding resonance or lock-on is also observed in 1991. Cope (1996), explains the compressibility acting to dampen flow field disturbances, the study's results indicate that quasi-periodic unsteady flow emerges from laminar, unsteady flow past a two-dimensional bluff body at low subsonic levels. Chan (2012), used two distinct computational fluid dynamic methods: the high-order spectral difference (SD) method, which was recently developed for compressible flow solution, and the Semi-Implicit Method for Pressure Linked Equation (SIMPLE), which is widely used in today's commercial incompressible flow solvers to study the behavior flow around the bluff bodies. In their work Zhang *et al.* (2014), the authors conduct simulations to assess the suitability of the standard k-ε turbulence model for engineering applications across subcritical to supercritical flow regimes. Gu *et al*. (2019), study Finite-Analytic Navier-Stokes (FANS) code is coupled with an in-house finite-element code to study the dynamic interaction between a floating buoy and its mooring system. Wu, Juliana, et al. introduce the effort to comprehend how the existence of a high void-fraction bubble mixture in the bluff body's near-wake affects the shedding dynamics for compressible flow, the effect of cavitation on the vortex shedding of bluff body wakes has been investigated Wu *et al*. (2021). Al-Haboobi *et al.* (2024), taking into account various Reynolds numbers (*Re*), used numerical studies to examine the flow patterns surrounding square and circular cylinders with equal length scale. A frequent event connected to fluid passing over an obstruction or the movement of a natural or artificial body is the flow over a bluff body. The flow across a bluff body is extremely viscous at considerably lower Reynolds numbers, and the force acting on the body is mostly due to skin friction. The vortex shedding occurs, though, when the Reynolds number rises over a critical point, which causes a large reduction in pressure on the body's back surface Choi *et al.* (2008). Improving our comprehension of the flow across yawed bluff bodies is the goal of this investigation.

The novelty of this work is using the Taylor-Galerkin/Pressure-Correction method to find the numerical solutions of incompressible Newtonian fluid flow around bluff bodies in an isothermal environment. Our algorithm was specifically developed to address fluid dynamics problems and serves as a tool to evaluate the effectiveness and accuracy of the applied method in solving compressible flow around circular and square bluff bodies. This problem is widely recognized as complex, and the successful testing of this method marks a significant achievement. The Taylor-Galerkin/Pressure-Correction method was initially introduced by Townsend and Webster. Consequently, this technique is used for compressible and incompressible flows that are both Newtonian and non-Newtonian. The two techniques used in this method are the pressure correction method and the Taylor Galerkin method. In the former (predictor-corrector), a two-step Lax-Wendroff time-stepping technique is employed, which is displayed in time via a Taylor series expansion. On the other hand, the latter broadens the compressibility requirement to guarantee second-order precision in time. Consequently, there has been a lot of interest in this approach for treating various flow issues (for more details you can see Al-Haboobi and Al-Muslimawi (2023), Fadhel and Al-Muslimawi (2022), Sharhan and Al-Muslimawi (2023)). The methodology employed in the solution when $\vartheta = \frac{1}{2}$ (Crank-Nicolson parameter) is the Crank-Nicolson approach, which decreases temporal errors in the time-stepping scheme and has higher precision and stability than other approaches Jin *et al.* (2017). Newton's second rule of motion for fluids may be compared to the Navier-Stokes equation, a nonlinear partial differential equation that governors the motion of actual fluids Bistafa (2018). These equations are considered among the most

important equations used to determine the behavior of compressible and incompressible fluids (governing equation).

The examples that are obvious include the wind blowing past a bridge and a tall structure, as well as the flows past a vehicle, a submarine, and an aero plane. As the topic of bluff body flow has been extensively studied by many researchers, rather than being based solely on empirical knowledge. Although the amount of knowledge that has been gathered is tremendous and the descriptive understanding that has been gained has yielded numerous discoveries, the process of moving towards a ``solution'' to the fundamental issue has been sluggish. This article will review a number of bluff body behaviors and their effect on fluid flow.

2. Mathematical modeling

The conservation laws of mass and momentum for compressible Newtonian flows under isothermal condition can be written as Al-Haboobi and Al-Muslimawi (2023), Kaushik (2022), Lukaszewicz and Kalita (2016)

$$\frac{\partial \rho}{\partial t} + Re\, \nabla \cdot (\rho v) = 0 \tag{1}$$

$$\rho Re \left(\frac{\partial v}{\partial t} + (v \cdot \nabla)v\right) = \nabla \cdot (2\mu d) - \frac{2}{3}\nabla(\mu \nabla \cdot v) - \nabla p \tag{2}$$

with ρ , p, v and μ represent fluid density, pressure, velocity vector and viscosity of fluid, respectively. Also, the rate of deformation tensor d is defined as $d = \frac{1}{2}\left(\nabla v + \nabla v^{\dagger}\right)$.[1] The Reynolds number *Re* which is non-dimensional number, defined by: Al-Haboobi and Al-Muslimawi (2023)

$$^{2}Re = \frac{\rho^{0}\, V^{0}\, L}{\mu} \tag{3}$$

The important point in this study is made relationship between pressure and density by using an equation of state (modified Tait equation of state Dymond and Malhotra (1988)) to build up the integrated system of governing equations. Here, the Tait formulation can be written as

$$\frac{p+B}{p_0+B} = \left(\frac{\rho}{\rho_0}\right)^{m} \tag{4}$$

where, m and B are parameters and ρ, ρ_0 represent reference values for pressure and density, respectively. By differentiating Eq. (4) with respect to ρ, we get

$$\frac{\partial p}{\partial \rho} = m\rho^{m-1}\frac{p_0+B}{\rho_0^{m}} = \frac{m(p+B)}{\rho} = c_{(x,t)}^{2} \tag{5}$$

$$\frac{\partial \rho}{\partial t} = \frac{\partial \rho}{\partial p}\frac{\partial p}{\partial t} = \frac{1}{c_{(x,t)}^{2}}\frac{\partial p}{\partial t} \tag{6}$$

---

[1]† represents tensor transpose.

[2]ρ^{0}, V^{0}represent density and velocity reference.

Where $c_{(x,t)}$ represents the speed of sound. By using the chain rule, we get,

3. Numerical technique

To address the system of compressible Newtonian fluids with isothermal conditions, we utilized the (TG/PC)-method. This Taylor-Galerkin based algorithm employs a fractional step method, initially semi-discretized in the time domain through Taylor's series time expansion and a pressure correction procedure. Developed by Hawken *et al.* this numerical approach was originally designed to tackle the challenges posed by incompressible isothermal flows Hawken *et al.* (1990). The Lax-Wendroff time stepping method (TG-M) is derived from the Taylor series expansion of time in two steps Donea (1984), Zienkiewicz *et al*. (1985).

Conservation of momentum equation becomes

$$\begin{aligned} &\text{step 1:} \quad \frac{2\rho Re}{\Delta t}\left[v^{n+\frac{1}{2}} - v^{n}\right] = G(v^{n}, d^{n}) - \nabla p^{n}, \\ &\text{step 2 :} \quad \frac{\rho Re}{\Delta t}[v^{n+1} - v^{n}] = G\left(v^{n+\frac{1}{2}}, d^{n+\frac{1}{2}}\right) - \nabla p^{n+\frac{1}{2}} \end{aligned} \tag{7}$$

where,

$G(v,d) = \nabla \cdot (2\mu d) - \frac{2}{3}\nabla(\mu \nabla \cdot v) - \rho Re(v \cdot \nabla)v.$

The pressure $p^{n+\frac{1}{2}}$ in Eq. (7 (step 2)) is approximated by

$$p^{n+\frac{1}{2}} = \vartheta p^{n+1} + (1-\vartheta)p^{n} \tag{8}$$

In this instance, the pressure $p^{n+1/2}$ has an error equal to $O(\Delta t^2)$ for $\vartheta = \frac{1}{2}$ while having an error equal to $O(\Delta t)$ for other values of ϑ, $p^{n+1/2}$. The Eq. (7 (step2)) can thus be expressed as

$$\frac{\rho Re}{\Delta t}[v^{n+1} - v^{n}] = G\left(v^{n+\frac{1}{2}}, d^{n+\frac{1}{2}}\right) - \vartheta \nabla p^{n+1} + (1-\vartheta)\nabla p^{n} \tag{9}$$

We propose a velocity v^{*} to solve Eq. (9) in conjunction with the compressibility Eq. (1), such that

$$\frac{\rho Re}{\Delta t}[v^{*} - v^{n}] = G\left(v^{n+\frac{1}{2}}, d^{n+\frac{1}{2}}\right) - \nabla p^{n} \tag{10}$$

Now, by subtracting Eq. (10) from Eq. (9), we obtain

$$\frac{\rho Re}{\Delta t}[v^{n+1} - v^{*}] = -\vartheta \nabla (p^{n+1} - p^{n}) \tag{11}$$

Using Eq. (1) and the divergence of the two sides of Eq. (11), we obtain

$$\frac{\Delta \rho^{n+1}}{\Delta t} + \nabla \cdot (\rho Re v^{*}) = \vartheta \Delta t \nabla^{2}(p^{n+1} - p^{n}) \tag{12}$$

Additionally, by using the chain rule to Eq. (5) and performing difference operations, we can connect the increase in density to the increase in pressure by

$$\frac{\Delta \rho^{n+1}}{\Delta t} = \frac{1}{c^{2}_{(x,t)}} \frac{\Delta p^{n+1}}{\Delta t} \tag{13}$$

Substituting Eq. (13) into Eq. (12), we have

$$\frac{1}{c^2_{(x,t)}}\frac{\Delta p^{n+1}}{\Delta t} + \nabla\cdot(\rho Re v^*) = \vartheta\Delta t\nabla^2(p^{n+1}-p^n) \tag{14}$$

Thus, from Eqs. (7(step 1)), (10), (11), (13) and (14), we can solve the system of compressible (mass and momentum) equations in the following order

$$\text{stage 1: } \frac{2\rho^n Re}{\Delta t}\left[v^{n+\frac{1}{2}} - v^n\right] = G(v^n, d^n) - \nabla p^n \tag{15}$$

$$\text{stage 2: } \frac{\rho^n Re}{\Delta t}[v^* - v^n] = G\left(v^{n+\frac{1}{2}}, d^{n+\frac{1}{2}}\right) - \nabla p^n \tag{16}$$

$$\text{stage 3: } \frac{1}{c^2_{(x,t)}}\frac{\Delta p^{n+1}}{\Delta t} + \nabla\cdot(\rho^n \operatorname{Re} v^*) = \vartheta\Delta t\nabla^2(p^{n+1}-p^n) \tag{17}$$

$$\text{stage 4: } \frac{\Delta\rho^{n+1}}{\Delta t} = \frac{1}{c^2_{(x,t)}}\frac{\Delta p^{n+1}}{\Delta t} \tag{18}$$

$$\text{stage 5: } \frac{\rho^n Re}{\Delta t}[v^{n+1} - v^*] = -\vartheta\nabla(p^{n+1}-p^n) \tag{19}$$

The matrix-vector representation of these stages can be explained as follows

$$\text{stage 1: } \frac{2\rho^n Re}{\Delta t}M\Delta V^{n+1/2} = L^\dagger P^n - \mu S V^n + \frac{2}{3}\mu D V^n - \rho^n\, Re\, N(V^n)V^n + \varpi \tag{20}$$

$$\text{stage 2: } \frac{\rho^n Re}{\Delta t}M\Delta V^* = L^\dagger P^n - \mu S V^{n+\frac{1}{2}} + \frac{2}{3}\mu D V^{n+\frac{1}{2}} - \rho^n R\, e\, N\left(V^{n+\frac{1}{2}}\right)V^{n+\frac{1}{2}} + \varpi \tag{21}$$

$$\text{stage 3: } \frac{1}{c^2_{(x,t)}}\frac{1}{\Delta t}H\Delta p^{n+1} + \rho^n Re\ CV^* = -\vartheta\Delta t K(P^{n+1}-P^n) \tag{22}$$

$$\text{stage 4: } \frac{1}{\Delta t}H\Delta\rho^{n+1} = \frac{1}{c^2_{(x,t)}}\frac{1}{\Delta t}H\Delta p^{n+1} \tag{23}$$

$$\text{stage 5 : } \frac{\rho^n Re}{\Delta t}M\Delta V^{n+1} = \vartheta L^\dagger(P^{n+1}-P^n) \tag{24}$$

where, $\Delta V^{n+1/2} = V^{n+1/2} - V^n, \Delta V^{n+1} = V^{n+1} - V^*, \Delta p^{n+1} = p^{n+1} - p^n$, $\Delta\rho^{n+1} = \rho^{n+1} - \rho^n$ and $\Delta V^* = V^* - V^n$. V is the velocity vector, ρ is the density vector and P is a pressure vector.

The notation and structure of matrix have been delineated as below

$$M_{ij} = [\phi_i, \phi_j] = \int_\Omega \phi_i\phi_j d\Omega,\ L_{ij} = (\psi_i, \nabla\cdot\phi_j) = \int_\Omega \psi_i\nabla\cdot\phi_j d\Omega,$$

$$S_{ij} = \left\langle\nabla\phi_i, \nabla\phi_j + (\nabla\phi_j)^\dagger\right\rangle = \int_\Omega \nabla\phi_i{:}\left(\nabla\phi_j + (\nabla\phi_j)^\dagger d\Omega,\right.$$

$$D_{ij} = [\nabla\phi_i, \nabla\phi_j] = \int_\Omega \nabla\phi_i\cdot\nabla\phi_j d\Omega,\ K_{ij} = [\nabla\psi_i, \nabla\psi_j] = \int_\Omega \nabla\psi_i\cdot\nabla\psi_j d\Omega,$$

$$H_{i,j} = (\psi_i, \psi_j) = \int_\Omega \psi_i\psi_j d\Omega,\ C_{ij} = \left(\psi_i, \nabla\cdot(\psi_j\phi_j)\right) = \int_\Omega \psi_i\nabla\cdot(\psi_j\phi_j)d\Omega,$$

$$N(V)_{ij} = [\phi_i, v\cdot\nabla\phi_j] = \int_\Omega\left(\sum_l \phi_i\phi_j V^t\cdot\nabla\right)\phi_j d\Omega,$$

$$\varpi_i = [\phi_i, f]_\Gamma = \int_\Gamma f\cdot\phi_i d\Gamma$$

Here, ϖ represents a natural boundary condition vector, and f is a given function.

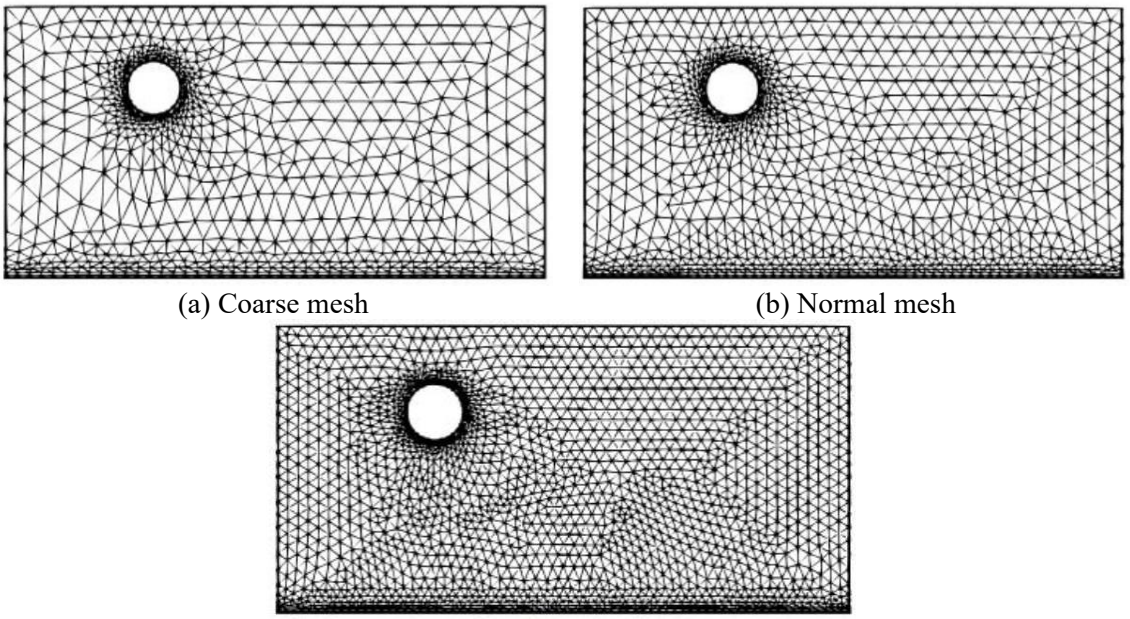

(a) Coarse mesh (b) Normal mesh

(c) Fine mesh

Fig. 1 Mesh Configuration with circular bluff bodies

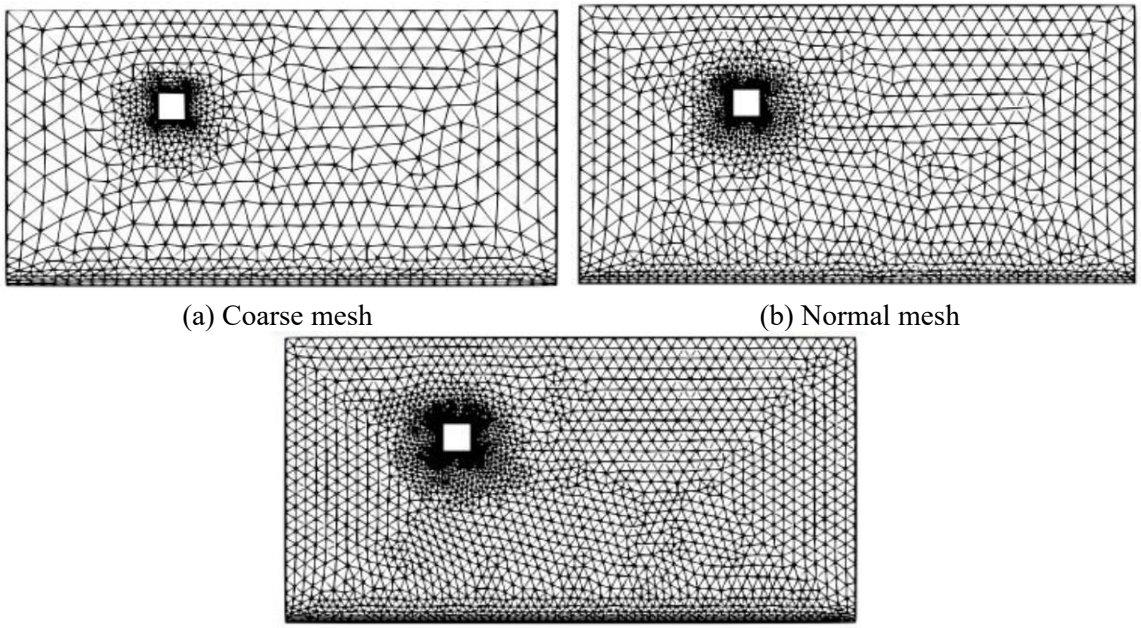

(a) Coarse mesh (b) Normal mesh

(c) Fine mesh

Fig. 2 Mesh Configuration with square bluff bodies

Table 1 Type of generated meshes

Mesh	Total Elements	Number of vertices	Degrees of freedom
		Circular shape	
Coarse	1506	885	2655
Normal	2115	1214	3642
Fine	3749	2073	6219
		Square shape	
Coarse	1736	998	2994
Normal	2739	1537	4611
Fine	4803	2617	7851

4. The problem and boundary conditions

In this section, we explore a benchmark problem centred on Newtonian compressible flow in a two-dimensional axisymmetric rectangular channel, specifically investigating compressible flow exhibiting Poiseuille (*Ps*) flow within this channel. The channel is characterized by a length L = 10 and a height H = 5, and it includes bluff bodies. To augment our analysis, we have employed three distinct triangular finite element meshes, each with different levels of refinement— coarse, normal, and fine, as depicted in Figs. 1 and 2. A comprehensive description of the attributes of this finite element meshes is provided in Table 1. All the results in this investigation are based on a fine mesh.

The velocity and pressure boundary conditions for the investigated problem are established as follows:

1) At the inlet, we prescribed a particular Poiseuille flow profile denoted as (*Ps*), in accordance with analytical expressions for fully-developed axial velocity, represented as $v_z = v_{max}(1 - (r^2/H^2))$. For further elaboration, please refer to White (2015).
2) No-slip boundary conditions (*BCs*) are enforced for velocity on the top wall of the channel.
3) No-slip boundary conditions (*BCs*) for velocity are imposed on the bluff bodies (for both circular and square).
4) Along the channel's outlet, we enforce zero radial velocity and pressure.

5. Numerical results

The subject of flow through channel with bluff bodies represent remains a significant challenge numerically. Thus, a Taylor-Galerkin/Pressure-Correction (TG/PC) method is nominated in the present study to face the difficulties of such problem due to of its high efficiency. Viscosity in the compressible flow under isothermal condition plays a fundamental role in terms of its effect on the essential components of fluid. Consequently, our research centers on elucidating the variations in viscosity and their impact on solution components, including fluid velocity (v), pressure (p), shear stress (τ_{rz}), radial stress (τ_{rr}), normal stress (τ_{zz}), shear-rate (ζ), strain-rate (Σ), and first normal stress (N_1). So, a comprehensive study of the effect of viscosity is presented with a

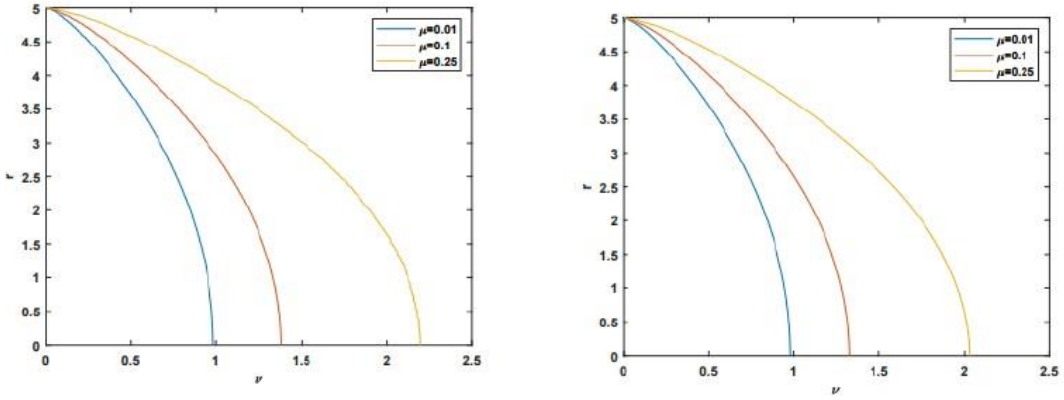

(a) Compressible circular bluff body (b) Compressible square bluff body

Fig. 3 Comparing the influence of various (μ) values on axial velocity with circular and square bluff bodies

comparison between two bluff body configurations (circular and square) in both incompressible and compressible flows. Furthermore, a fine grid will be uniformly applied to all the outcomes under investigation.

(μ)-variation: In Fig. 3, the axial velocity within the full channel development region is depicted for various viscosities in compressible flows around both circular and square bluff bodies. These plots illustrate the discernible influence of viscosity, particularly in compressible flows. This heightened effect of viscosity in compressible flows arises from the alterations in density of fluids resulting from viscosity levels, directly impacting the dynamics of compressible flow.

The findings underscore the high accuracy of results across a viscosity range of $0.01 \leq \mu \leq 0.1$. Nevertheless, for viscosities exceeding 0.1, there is a degree of variation. This behavior can be ascribed to the characteristics of (Ps), where the velocity resides within the range of $0.9 < \nu < 1.4$. Notably, it is observed that the influence of an imaginary circular body induces a more significant alteration in velocity compared to a square body, as evident in Fig. 3(a). These outcomes align with the findings presented in Al-Haboobi and Al-Muslimawi (2023).

Fig. 4 illustrates the relationship between viscosity and pressure. The profiles demonstrate that as viscosity increases, so does the pressure, primarily because of the heightened molecular attraction forces. Noticeable that, this increase is more pronounced and evident in the compressible situation compared to incompressible. Regarding to a bluff body influence, we notice an obviously reduction in the level of pressure, which reflects a phenomenon akin to the creation of a vacuum.

This occurs because the presence of a hollow object in the fluid flow leads to flow separation and the formation of a low-pressure vacuum zone. Moreover, the low-pressure zone becomes more conspicuous as the viscosity of fluid rises due to delayed flow separation and increased dissipation of energy, as shown in Achenbach (1972). Additionally, when referring to Figs. 4(a) and 4(c), it becomes evident that the vacuum effect is more pronounced when the bluff body has a circular shape compared to a square. The state equation of density is basically formulated based on pressure, so viscosity also has a comparable effect on density. Fig. 5 displays that how increasing viscosity affects density and provides a comparative analysis between circular and square bluff bodies.

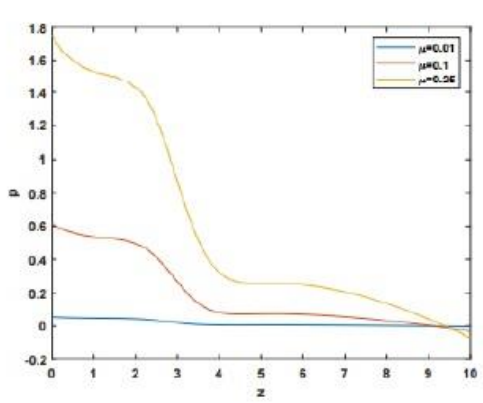

(a) Compressible circular bluff body

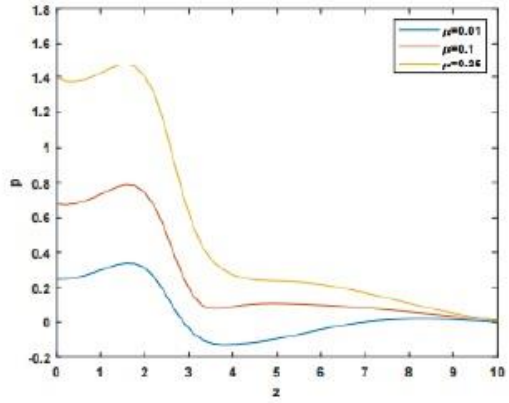

(b) Incompressible circular bluff body

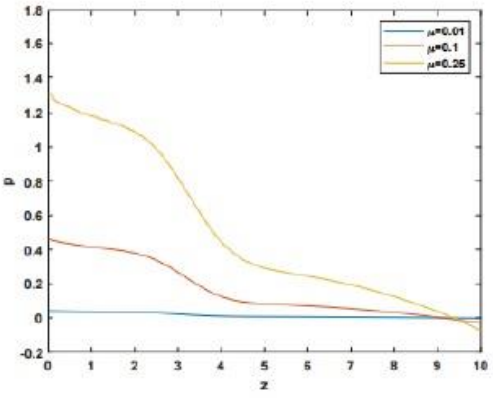

(c) Compressible square bluff body

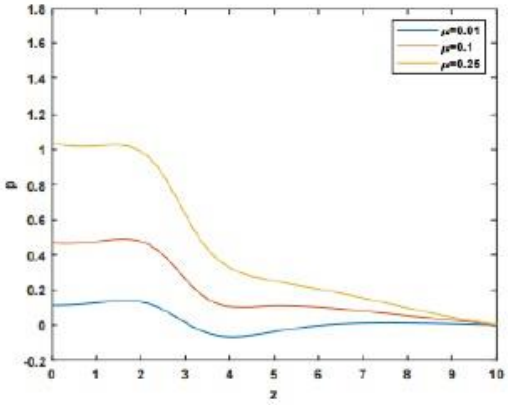

(d) Incompressible square bluff body

Fig. 4 Comparing the influence of various (μ) values on pressure drop with circular and square bluff bodies

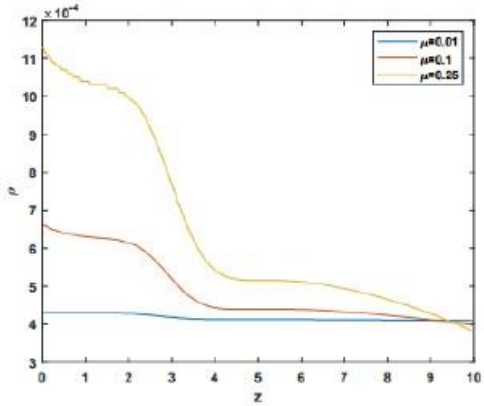

(a) Compressible circular bluff body

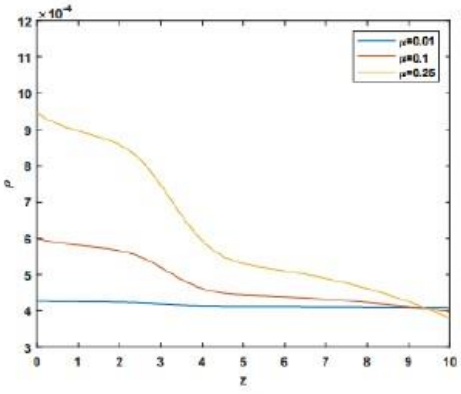

(b) Incompressible circular bluff body

Fig. 5 Comparing the influence of various (μ) values on density with circular and square bluff bodies

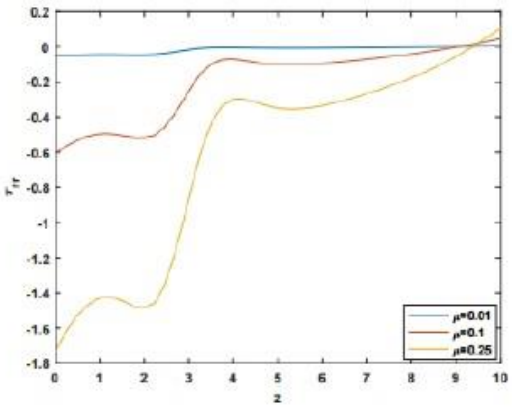

(a) Compressible circular bluff body

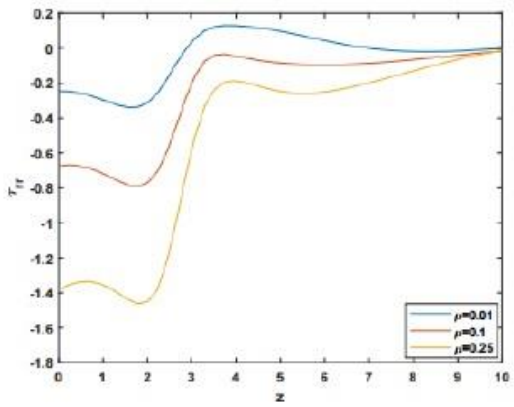

(b) Incompressible circular bluff body

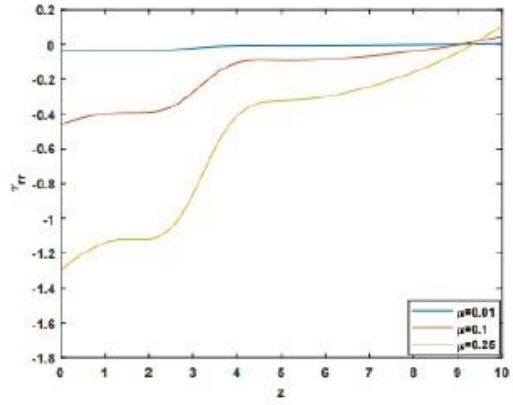

(c) Compressible square bluff body

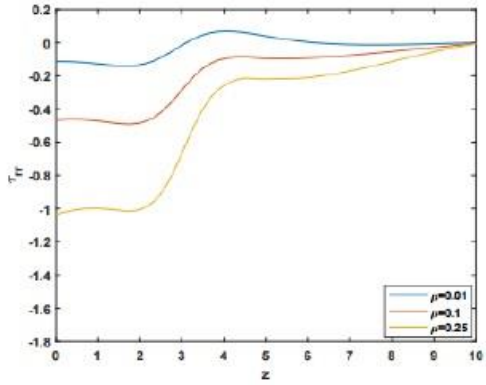

(d) Incompressible square bluff body

Fig. 6 Comparing the influence of various (μ) values on normal stress (τ_{rr}) with circular and square bluff bodies

In addition to the above results, we explore the effects of viscosity and the existence of bluff bodies on radial stress (τ_{rr}) and normal stress (τ_{zz}). Here, the profiles of these stresses along the centerline of the channel is plotted for three different mu-values ($\mu = \{0.01, 0.1, 0.25\}$). Findings reveal that, there is a pronounced increase in magnitude of both stresses with rising viscosity. This phenomenon can be attributed to the enhanced resistance of the fluid to shear deformation, as referenced in Currie (2016). With respect to the role of bluff bodies, a notable peak is discernible around these the location of bodies (between $z = 1$ and $z = 3$). Moreover, as the viscosity increases, there is a marked amplification in turbulence, resulting in elevated pressure levels. Physically, this surge in pressure, in turn, creates a more substantial vacuum, further intensifying the turbulence. Additional comparative analysis between compressible and incompressible cases in both circular bluff body and square bluff body are presented as well. Indeed Fig. 6 illustrates two important comparisons. Firstly, comparison between the compressible and incompressible cases is conducted. In this context, viscosity has a modest effect on (τ_{rr}) in the compressible flow compared to incompressible, with a few increases in magnitude for compressible flow.

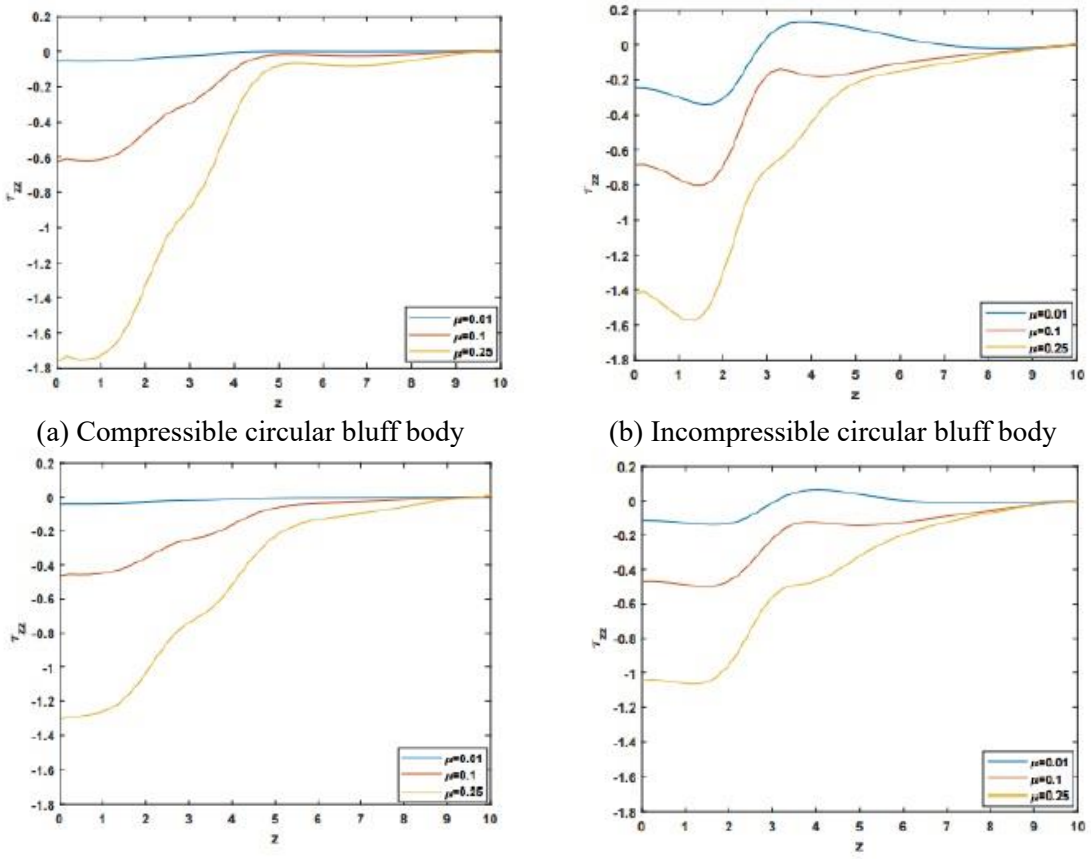

(a) Compressible circular bluff body (b) Incompressible circular bluff body

(c) Compressible square bluff body (d) Incompressible square bluff body

Fig. 7 Comparing the influence of various (μ) values on normal stress (τ_{rr}) with circular and square bluff bodies

The second comparison pertains to the presence of circular and square bluff bodies, where through the radial component (τ_{rr}), we note slight increase in magnitude in the case of existence circular bluff body compared to that in square bluff body situation.

Additionally, interesting comparison in normal stress (τ_{zz}) between incompressible and compressible flows is shown in Fig. 7 in both situations of bluff bodies. Generally, and in the line with the observed stresses results, we notice an increase in the normal stress magnitude in the case of compressible flows compared to that with incompressible, specially for the presence of a circular bluff body.

Next, we analyses shear stress (τ_{rz}) and shear-rate (ζ) along the top wall of the channel ac-cording to different level of viscocity for both (circular bluff/square bluff)-incompressible and (circular bluff/square bluff)-compressible. In all cases, there is an evident impact of the viscosity on the (τ_{rz}) and (ζ), with consistent relationship between them as illustrated in Figs. 8 and 9 Plawsky (2014). The profiles demonstrate that, as viscosity increases, the magnitude of (τ_{rz}) and (ζ) increases, with slightly less in the case of incompressible. In this context, regards to the influenceof bluff bodies, a distinct peak is discernible in the vicinity of these bodies, particularly between $z = 1$ and $z = 3$. Furthermore, the

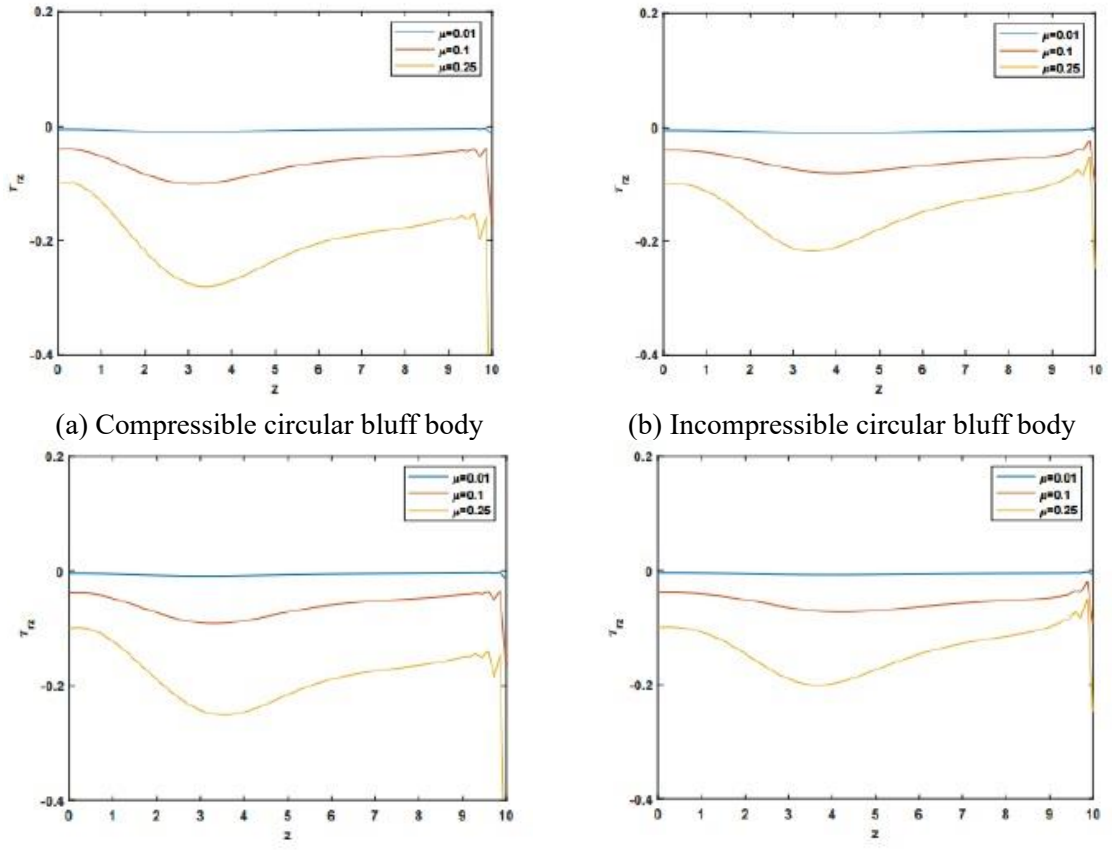

(a) Compressible circular bluff body (b) Incompressible circular bluff body

(c) Compressible square bluff body (d) Incompressible square bluff body

Fig. 8 Comparing the influence of various (μ) values on shear stress (τ_{rz}) with circular and square bluff bodies

increase in viscosity amplifies turbulence, resulting in elevated pressure levels. This surge in pressure consequently results in a more significant vacuum effect. Moreover, the outcomes closely align with those observed in (τ_{rr}) and (τ_{zz}), reinforcing the notion that the effect is more pronounced when the fluid is in a compressible state and when a circular bluff body is introduced.

By using a same setting of parameters, we observed impact of increasing viscosity on both the st-rain-rate (Σ) and the first normal stress $(N_1 = \tau_{zz} - \tau_{rr})$, through the centerline of channel. Asdepicted in Figs. 10 and 11, a rise in viscosity leads to an increase in (Σ) and (N_1) for both inc-ompressible (circular bluff/square bluff) and compressible (circular bluff/square bluff), with noti-ceable disruptions in the areas surrounding the bluff bodies. Notably, the turbulence intensifiesaroudcircular bluff bodies, a consequence of distinct flow separation behaviors, as detailed in Chang (2014), Simpson (1981).

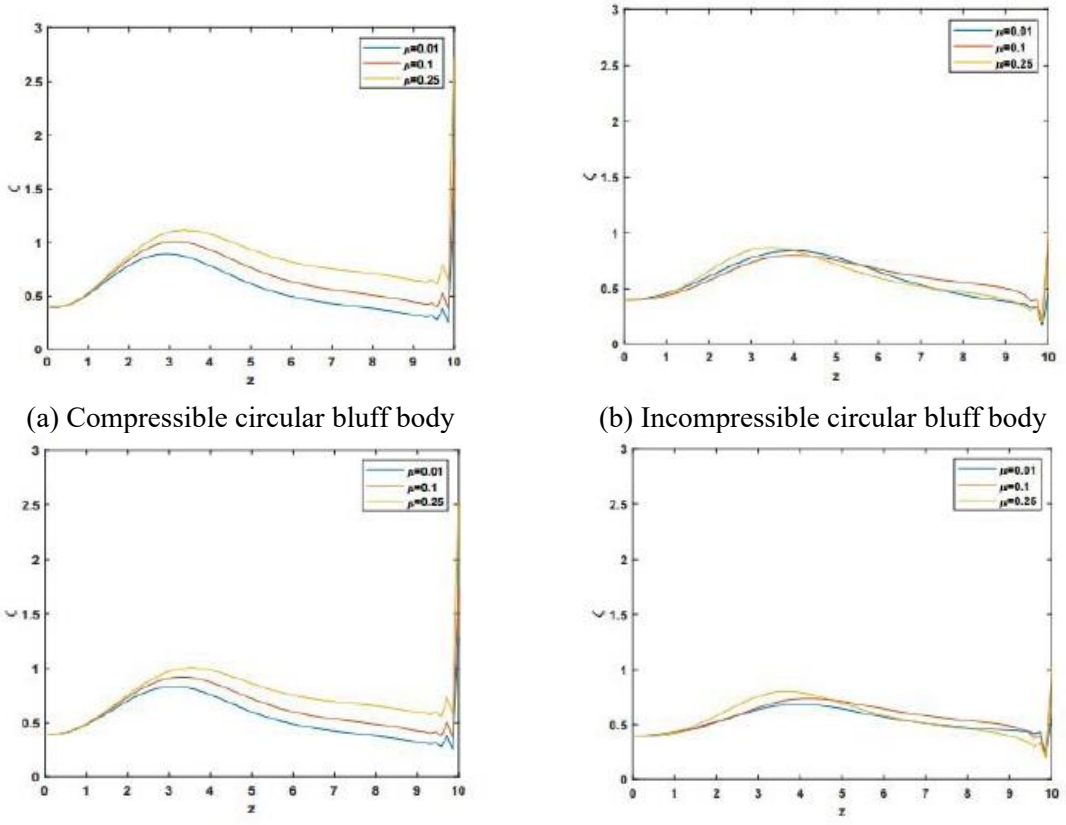

(a) Compressible circular bluff body (b) Incompressible circular bluff body

(c) Compressible square bluff body (d) Incompressible square bluff body

Fig. 9 Comparing the influence of various (μ) values on shear-rate (ζ) with circular and square bluff bodies

6. Conclusions

This investigation utilized numerical simulations to analyze the flow patterns of compressible Newtonian fluids around square and circular bluff bodies with equivalent characteristic length scales, while considering varying viscosities (μ). The (TG/PC)-method, was employed to examine the impact of bluff bodies. The determination of density (\rho) involved incorporating the relationship between density and pressure, as dictated by the equation of state, into the method. Through this method, the study assessed the influence of viscosity (μ) on various fluid properties, including velocity (v), pressure (p), density (ρ), shear stress (τ_{rz}), radial stress (τ_{rr}), normal stress (τ_{zz}), shear-rate (ζ), strain-rate (Σ), and first normal stress (N_1). The outcomes revealed a direct correlation between viscosity, velocity, pressure, density, shear-rate, and strain-rate, as well as first normal stress, while an inverse relationship was observed with radial stress, normal stress, and shear stress. Additionally, the study highlighted on the discernible impact of the bluff body's shape on the obtained results. In general, the performed tests produced highly satisfactory results, closely aligning with the expected physical behavior.

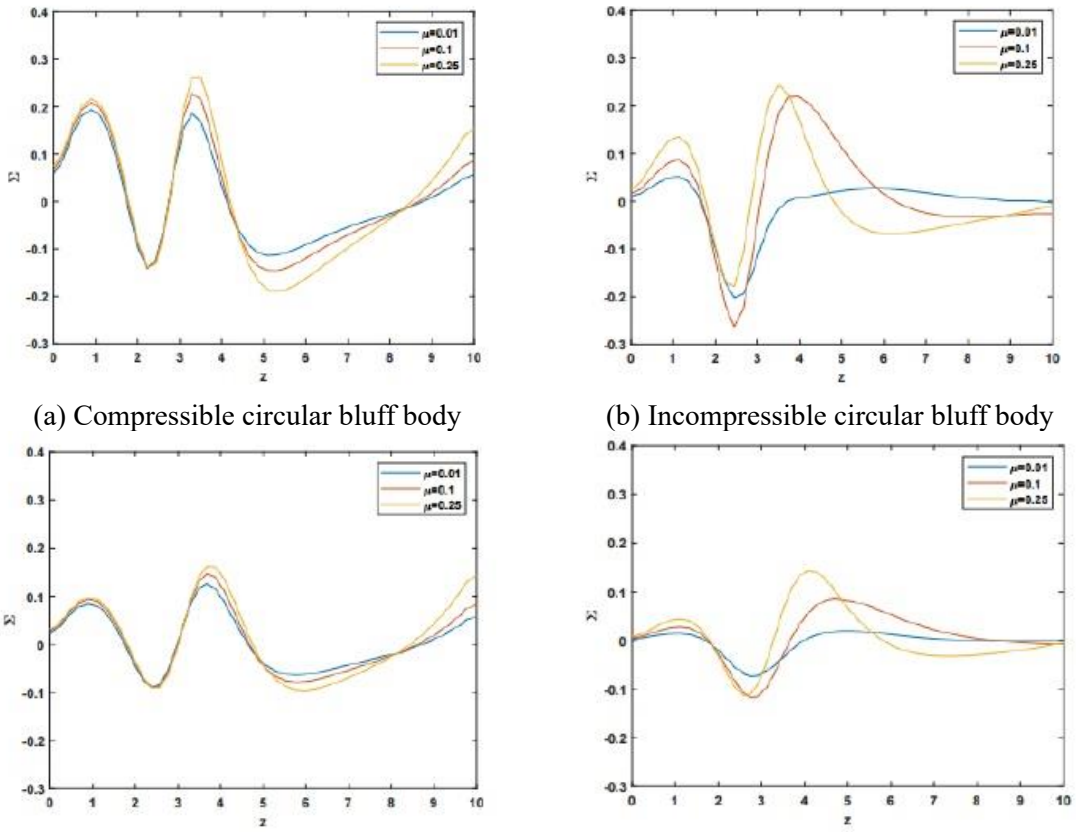

(a) Compressible circular bluff body (b) Incompressible circular bluff body

(c) Compressible square bluff body (d) Incompressible square bluff body

Fig. 10 Comparing the influence of various (μ) values on shear-rate (Σ) with circular and square bluff bodies

References

Achenbach, E. (1972), "Experiments on the flow past spheres at very high reynolds numbers", *J. Fluid Mech.*, **54**(3), 565-575. https://doi.org/10.1017/S0022112072000874.

Al-Haboobi, A., Al-Juaifri, G.A. and Al-Muslimawi, A.H. (2024), "Numerical study of newtonian laminar flow around circular and square cylinders", *Results Control Optim.*, **14**, 100328. https://doi.org/10.1016/j.rico.2023.100328.

Al-Haboobi, A. and Al-Muslimawi, A.H. (2023), "Novel algorithm for compressible newtonian axisymmetric thermal flow", *Int. J. Modern Phys. C*, 2450025. https://doi.org/10.1142/S0129183124500256.

Bimbato, A.M., Alcntara Pereira, L.A. and Hirata, M.H. (2011), "Study of the vortex shedding flow around a body near a moving ground", *J. Wind Eng. Ind. Aerod.*, **99**(1), 7-17. https://doi.org/10.1016/j.jweia.2010.10.003.

Bistafa, S.R. (2018), "On the development of the navier-stokes equation by navier", *Revista Brasileira de Ensino de Fisica*, **40**(2). https://doi.org/10.1590/1806–9126–RBEF–2017–0239.

Chan, A.S. (2012), Control and Suppression Of Laminar Vortex Shedding Off Two-Dimensional Bluff Bodies. Stanford University.

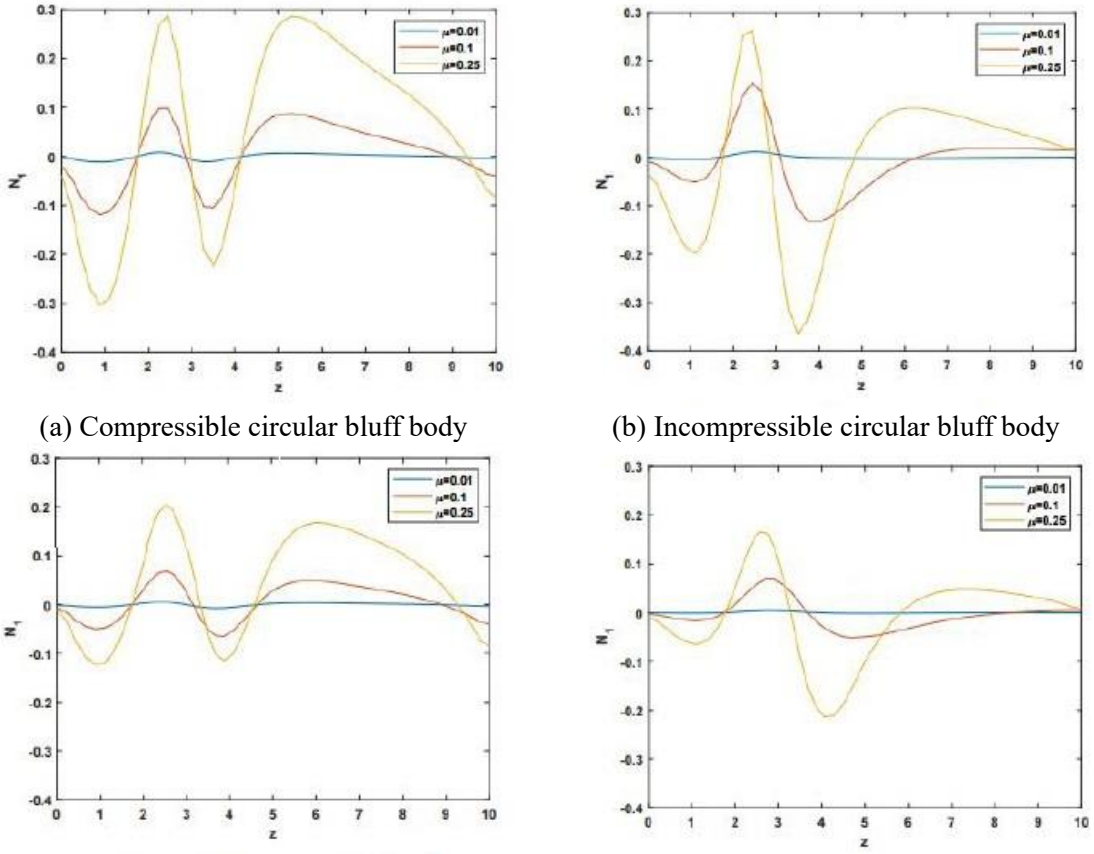

(a) Compressible circular bluff body (b) Incompressible circular bluff body

(c) Compressible square bluff body (d) Incompressible square bluff body

Fig. 11 Comparing the influence of various (μ) values on first normal stress (N_1) with circular and square bluff bodies

Chang, P.K. (2014), Separation of Flow. Elsevier.

Choi, H., Jeon, W.P. and Kim, J. (2008), "Control of flow over a bluff body", *Annu. Rev. Fluid Mech.*, **40**, 113-139. https://doi.org/10.1146/annurev.fluid.39.050905.110149.

Cope, W.K. (1996), A study of compressibility effects on Laminar, Unsteady flow past a two-dimensional bluff body. University of Illinois at Urbana-Champaign.

Currie, I. (2016), Fundamental mechanics of fluids, 4th Ed., CRC Press, USA.

Donea, J. (1984), "A taylor–galerkin method for convective transport problems", *Int. J. Numer. Method. Eng.*, **20**(1), 101-119. https://doi.org/10.1002/nme.1620200108.

Dymond, J. and Malhotra, R. (1988), "The tait equation: 100 years on", *Int. J. Thermophys.*, **9**(6), 941-951. https://doi.org/10.1007/BF01133262.

Fadhel, I.A. and Al-Muslimawi, A.H. (2022), "Numerical simulation of stick-slip viscoelastic fluid by using a hybrid finite-element/volume method", **2398**, 060045. https://doi.org/10.1063/5.0093620.

Griffin, O.M. and Hall, M.S. (1991), "Review–vortex shedding lock-on and flow control in bluff body wakes", *J. Fluid. Eng.*, **113**(4), 526-537. https://doi.org/10.1115/1.2926511.

Gu, H., Chen, H.C. and Zhao, L. (2019), "Coupled cfd-fem simulation of hydrodynamic responses of a calm buoy", *Ocean Syst. Eng.*, **9**(1), 21-42. https://doi.org/10.12989/ose.2019.9.1.021.

Hawken, D., Tamaddon-Jahromi, H., Townsend, P. and Webster, M. (1990), "A taylor–galerkin–based algorithm for viscous incompressible flow", *Int. J. Numer. Method. Fl.*, **10**(3), 327-351. https://doi.org/10.1002/fld.1650100307.

Jin, B., Li, B. and Zhou, Z. (2017), "An analysis of the Crank–Nicolson method for subdiffusion", *IMA J. Numer. Anal*., **38**(1), 518-541. https://doi.org/10.1093/imanum/drx019.

Kaushik, M. (2022), "Governing equations and thermodynamics of compressible flows", *Fundament. Gas Dynam*., 47-107.

Lukaszewicz, G. and Kalita, P. (2016), "Navier–stokes equations", **34**, Springer, Switzerland.

Plawsky, J.L. (2014), "Transport phenomena fundamentals", 3rd Ed., CRC Press, USA. https://doi.org/10.1201/9781439882122.

Sharhan, A. and Al-Muslimawi, A. (2023), "Inelastic solution for power law fluid with taylor galerkin-pressure correction finite element method: Axisymmetric contraction flows", *J. Appl. Fluid Mech*., **16**(12), 2411-2423. https://doi.org/10.47176/jafm.16.12.1982.

Simpson, R. (1981), "A review of some phenomena in turbulent flow separation", *J. Fluid. Eng. T. ASME* **103**(4), 520-533. https://doi.org/10.1115/1.3241761.

White, F.M. (2015), Fluid mechanics. The McGraw Hill Companies.

Wu, J., Deijlen, L., Bhatt, A., Ganesh, H. and Ceccio, S.L. (2021), "Cavitation dynamics and vortex shedding in the wake of a bluff body", *J. Fluid Mech*., **917**, 26. https://doi.org/10.1017/jfm.2021.263.

Zhang, X.T., Li, Z.Y., Fu, S.X., Ong, M.C. and Chen, Y. (2014), "Study of the flow around a cylinder from the subcritical to supercritical regimes", *Ocean Syst. Eng*., **4**(3), 185-200. https://doi.org/10.12989/ose.2014.4.3.185.

Zienkiewicz, O., Morgan, K., Peraire, J., Vandati, M. and Löhner, R. (1985), "Finite elements for compressible gas flow and similar systems", *Proceedings of the 7th Int. Conf. Comput. Meth. Appl. Sci. Eng*.

MK